batteries

MDPI

Article

Agglomeration-Free and Air-Inert Garnet for Upgrading PEO/Garnet Composite Solid State Electrolyte

Jun Cheng [1,†], Hongqiang Zhang [1,†], Deping Li [1,*], Yuanyuan Li [1], Zhen Zeng [1], Fengjun Ji [1], Youri Wei [1], Xiao Xu [1], Qing Sun [1], Shang Wang [2], Jingyu Lu [3] and Lijie Ci [1,*]

[1] State Key Laboratory of Advanced Welding and Joining, School of Materials Science and Engineering, Harbin Institute of Technology (Shenzhen), Shenzhen 518055, China
[2] State Key Laboratory of Advanced Welding and Joining, Harbin Institute of Technology, Harbin 150001, China
[3] School of Science, Harbin Institute of Technology (Shenzhen), Shenzhen 518055, China
* Correspondence: lideping@hit.edu.cn (D.L.); cilijie@hit.edu.cn (L.C.)
† These authors contributed equally to this work.

Abstract: Due to the intrinsically high ionic conductivity and good interfacial stability towards lithium, garnet-type solid electrolytes are usually introduced into polymer electrolytes as fillers to prepare polymer/garnet composite electrolytes, which can improve the ionic conductivity and enhance the mechanical strength to suppress Li dendrites. However, the surface Li_2CO_3 and/or LiOH passive layers which form when garnet is exposed to the air greatly reduce the enhancement effect of garnet on the composite electrolyte. Furthermore, compared with micro-size particles, nano-size garnet fillers exhibit a better effect on enhancing the performance of composite solid electrolytes. Nevertheless, inferior organic/inorganic interphase compatibility and high specific surface energy of nanofillers inevitably cause agglomeration, which severely hinders the effect of nanoparticles for promoting composite solid electrolytes. Herein, a cost-effective amphipathic 3-Aminopropyltriethoxysilane coupling agent is introduced to modify garnet fillers, which effectively expands the air stability of garnet and greatly improves the dispersion of garnet fillers in the polymer matrix. The well-dispersed garnet filler/polymer interface is intimate through the bridging effect of the silane coupling agent, resulting in boosted ionic conductivity (0.72×10^{-4} S/cm at room temperature) of the composite electrolyte, enhanced stability against lithium dendrites (critical current density > 0.5 mA/cm^2), and prolonged cycling life of LFP/Li full cells.

Keywords: garnet solid electrolyte; composite solid electrolyte; air stability; solid state batteries

Citation: Cheng, J.; Zhang, H.; Li, D.; Li, Y.; Zeng, Z.; Ji, F.; Wei, Y.; Xu, X.; Sun, Q.; Wang, S.; et al. Agglomeration-Free and Air-Inert Garnet for Upgrading PEO/Garnet Composite Solid State Electrolyte. *Batteries* **2022**, *8*, 141. https://doi.org/10.3390/batteries8100141

Academic Editors: Guojin Liang, Funian Mo and Pascal Venet

Received: 3 August 2022
Accepted: 16 September 2022
Published: 23 September 2022

1. Introduction

In recent years, solid-state batteries (SSBs) have received extensive attention due to their intrinsic safety and theoretically high energy density [1–4]. As a key component of SSBs, various types of solid-state electrolytes (SSEs) have been inclusively studied for decades, such as sulfide-type, NASICON-type, and garnet-type [5–8]. Among them, garnet-type electrolyte $Li_7La_3Zr_2O_{12}$ (LLZO) is considered one of the most promising SSEs due to its excellent chemical/electrochemical stability against Li metal anode and high ionic conductivity [9–12]. Garnet solid electrolyte ceramics exhibit high ionic conductivity and excellent electrochemical stability, but their poor wettability with electrodes and difficulty in battery assembly hinder their commercial application [7,13–16]. Therefore, garnet-type electrolytes are also usually used as fillers for reinforced polymer solid electrolytes owing to their excellent electrochemical and chemical properties.

However, garnet-type electrolytes are unstable in air and react with H_2O and CO_2 to form LiOH and Li_2CO_3 passivation layer on its surface, reducing its effect on enhancing the performance of composite solid electrolytes [17–19]. This generated insulation layer (~10^{-8} S/cm at 200 °C) would change the surface chemical properties of LLZO particles and interrupt Li^+ transfer between the LLZO and PEO matrix, which hence will lead to sluggish

ion transport in assembled batteries. In addition, the Lewis-acid LLZO surface promotes the dissociation of lithium salts and the immobilization of lithium salt anions, which is hindered by the coverage of the passivation layer, resulting in low Li^+ concentration and high overpotential. Moreover, the high overpotential can act as the driving force to trigger Li dendrite growth and eventual short circuit of cells [20]. In addition, nano-size garnet electrolyte particles with a large specific surface area tend to agglomerate in the polymer electrolytes due to high surface energy and insufficient coordination number of surface atoms, which further hinders the enhancement effect of garnet electrolyte fillers on composite electrolyte [20]. Furthermore, in general, the difference in the surface energy of the two materials determines the wettability. The specific surface energy of LLZO is about 3 J/m^2, while the PEO is only about 44 mJ/m^2 [21]. The huge gap in specific surface energy causes poor wettability between PEO/LLZO. Therefore, improving the garnet fillers' stability in air and the dispersibility and wettability in the polymer matrix are of great importance for improving the performance of the garnet-based composite solid electrolyte.

Numerous research has been carried out to investigate the effect of LiOH and Li_2CO_3 passivation layer on electrolyte properties and provided several effective means to remove the passivation layer [17–20,22]. In addition, Jeff Sakamoto et al. [23] also proved a highly resistive PEO-LiTFSI (Lithium Bis(trifluoromethanesulphonyl)imide)/Li_2CO_3@LLZO interface, with a resistivity of 95 $k\Omega/cm^2$ (30 °C). By removing surface impurities through heat treatment, the $R_{interface}$ was reduced to 180 Ω/cm^2 at 30 °C. Huo et al. [22] obtained the Li_2CO_3-free LLZTO (Ta doped-LLZO) by high-temperature treatment (600 °C) under an Ar atmosphere. In addition, the Li_2CO_3-free LLZTO enhanced composite electrolyte exhibits an improved ionic conductivity of 5.5×10^{-5} S/cm at 25 °C and strengthens lithium dendrite suppression (600 h@0.2 mA/cm^2). Lee et al. [24] eliminated the resistive layers at the LLZO surface through reactive ion (CF_4) etching. The etched LLZO@polyvinylidene fluoride composite electrolyte exhibits a two-fold improvement in ionic conductivity from the non-etched counterpart. In addition, great effort has been devoted to improving the dispersion of nano-size garnets in polymer matrices [25–27]. Wang et al. applied dopamine to improve the wettability of LLZTO with polyethylene oxide (PEO), and the dispersion of LLZTO in the PEO was extremely improved after the polydopamine coating. With dopamine modification, the ionic conductivity of the composite electrolyte at 30 °C is doubled, and the interfacial resistance of the Li/composite electrolyte/Li symmetric cell decreased from 308 $\Omega \cdot cm^2$ to 65 $\Omega \cdot cm^2$ at 50 °C. Goodenough et al. [28] proposed LiF to prevent garnet electrolytes from moist air. The garnet LLZT-2 wt.%LiF with less Li_2CO_3 on the surface was proved to exhibit a small interfacial resistance with Li metal, a solid polymer electrolyte, and organic-liquid electrolytes. Moreover, the assembled all-solid-state Li/polymer/LLZT-2LiF/$LiFePO_4$ battery exhibits high coulombic efficiency and long cycle life. Great progress has been achieved in improving the garnet fillers' air stability or the dispersion in the polymer matrix until now [29]. However, the two-step operation of passivation layer removal and surface coating on the original LLZO filler is cumbersome. To achieve the commercial application of garnet-based composite solid electrolyte, it is necessary to explore a facile and cost-effective process to simultaneously increase the air stability of the garnet electrolyte and its dispersibility in the polymer substrate.

Herein, we provide a facile method to further upgrade the garnet composite electrolyte. $Li_{6.4}La_3Zr_{1.4}Ta_{0.6}O_{12}$ (Ta-LLZO) nanoparticles dispersion in the PEO matrix was improved by a facile silane coupling agent coating. The dual wetting ability of the silane coupling agent towards organic substrates and inorganic fillers allows it to act as a bridge to tightly connect LLZO and PEO, which effectively promotes the electrochemical performance of the composite electrolyte. In addition, the hydrophobic silane coupling agent coated LLZO shows better air stability when compared to pristine LLZO. The symmetric lithium batteries delivered prolonged cycling life at a high current density (0.5 mA/cm^2), and the assembled $LiFePO_4$ (LFP)/Li cells exhibited excellent cycle stability at 6 °C and room temperature.

2. Results and Discussion

It is well known that LiOH and Li_2CO_3 passivation layer will be formed on the surface of LLZO when it was exposed to the ambient air with the existence of moisture and CO_2 [20]. which hence will lead to a decrease in the effect of the garnet solid electrolyte to enhance the electrochemical performance of the composite solid electrolyte [1].

As illustrated in Figure 1, to remove the passivation layer, hydrochloric acid was adopted to react with LiOH and Li_2CO_3 on the surface of pristine LLZO (P−LLZO) (the obtained LLZO particle denoted H−LLZO). After removing the passivation layer, the KH550 silane coupling agent was used to modify the H−LLZO. The hydroxyl group on the surface of LLZO and the silyl hydroxyl group obtained by the hydrolysis of the silane coupling agent undergo a hydrolysis polycondensation reaction to realize the tight coating of the silane coupling agent on the surface of LLZO (the obtained LLZO particle is denoted as K−LLZO).

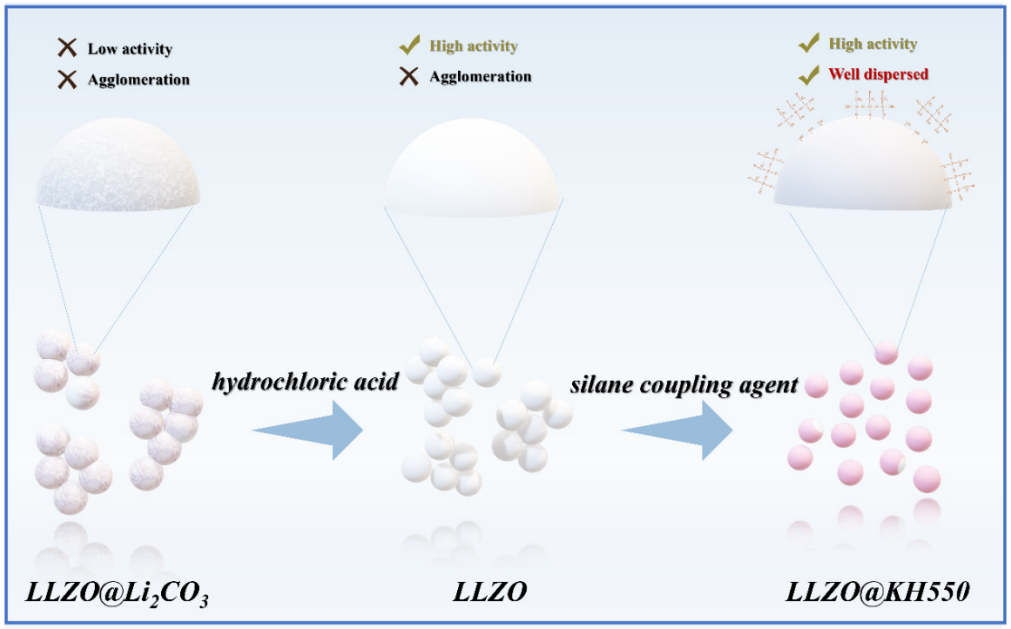

Figure 1. Schematic diagram of the process of coating LLZO with silane coupling agent KH550.

As is shown in Figure 2a, the peaks of P−LLZO X-ray diffraction (XRD) patterns at ~21° and 23° belong to LiOH and Li_2CO_3, respectively [30]. After the treatment with dilute hydrochloric acid, the peaks corresponding to LiOH and Li_2CO_3 vanished, which indicates the surface Li_2CO_3 and LiOH passivation layer of LLZO were completely removed. Besides, due to the less content of the surface coating layer, the XRD patterns of K−LLZO and H−LLZO show no significant difference after coating with a silane coupling agent, indicating that the coating process has no obvious effect on the phase structure of LLZO. In addition, the SEM images (Figure 2b–d) of different LLZO particle present the uniform and well-dispersed morphology of K−LLZO, superior to other samples. The above result suggests the coating of the coupling agent can effectively inhibit the agglomeration of LLZO particles, which may assist its subsequent dispersion in the polymer matrix. Furthermore, the surface SEM images of the composite electrolyte verified that the K−LLZO particles are evenly dispersed in the polymer matrix, while the P−LLZO particles in the control sample exhibit obvious agglomeration (Figure 2e,f). In general, the addition of active fillers can improve the ionic conductivity of composite electrolytes from three aspects: (i) The addition of active fillers can effectively interrupt the crystallization of PEO chains and increase the amorphous lithium-ion region; (ii) Active fillers naturally have lithium ionic conductivity can play the role of conducting lithium ions. (iii) The formation of a fast lithium-ion conduction channel at the interface between the active filler and the

polymer matrix promotes the rapid conduction of lithium ions [31–33]. Compared with the agglomerated P−LLZO, the well dispersed K−LLZO hinders the crystallization of PEO chains more effectively, and the well dispersed K−LLZO can provide a more specific surface area, which is conducive to the construction of polymers and active filler interface for fast lithium-ion conduction. Therefore, the K−LLZO@PEO (KLP) with well-dispersed K−LLZO is more likely to exhibit better electrochemical performance than P−LLZO@PEO (PLP). The FTIR and Raman spectroscopy were applied to further identify the Li-containing phases considering a low X-ray scattering factor for Li. spectra. The characteristic FTIR peak at 1415 cm^{-1} 1087 cm^{-1}, and 869 cm^{-1} of the P−LLZO sample attributes to ν(C=O), ν(C-O), and δ(C=O), respectively, which corresponds to the surface Li_2CO_3 passivation layer. Moreover, the peak at 3675 cm^{-1} (shadow highlight) conforms to the -OH of the LiOH passivation layer. After the treatment of hydrochloric acid, the reduced peak intensity demonstrates that the surface passivation layers have been greatly eliminated. Furthermore, the characteristic Raman peaks at 680 cm^{-1} and 770 cm^{-1} were ascribed to the cubic LLZTO phase, and the characteristic Raman peak of ν(C-O) and -OH at 1089 cm^{-1} and 3666 cm^{-1}, respectively, vanished after hydrochloric acid treatment. The results of FTIR and Raman spectra suggest that Li_2CO_3 and LiOH were greatly removed by the hydrochloric acid treatment based on reduced characteristic peaks. Furthermore, the FTIR peak at ~1200 cm^{-1} (shadow highlight) corresponds to the characteristic peak of ν(C-N) in the KH550 silane coupling agent, indicating that the silane coupling agent has been coated on the surface of LLZO. In addition, the Raman spectrum characteristic peak of K−LLZO at 900 cm^{-1} (shadow highlight) corresponds to δ(C-N), further proving the successful coating of the silane coupling agent (Figure 2g,h) [34]. Moreover, the EDS mapping images of K−LLZO in Supplementary Material Figure S1 also verified the silane coupling agent coating on LLZO. Moreover, after exposing K−LLZO and H−LLZO to the air for one month, the XRD patterns (Figures 2i and S2) of the K−LLZO sample reveal that no recognizable peaks of Li_2CO_3 and LiOH were observed, while the counter H−LLZO sample exhibits obvious peaks of the passivation layer, which shows that the silane coupling agent does play a critical role in improving the air stability of LLZO.

The Nyquist plots and calculated ionic conductivity of different filler contents PLP were displayed in Figure 3a,b, respectively. The small intercept corresponds to the electrolyte resistance (R_{ohm}), the depressed semicircle is related to the charge transfer resistance (R_{ct}) and the constant phase element, and the inclined line at low frequencies represents the Warburg impedance due to the diffusion of lithium ions in the electrode (Z_w). Obviously, 20 wt.% PLP exhibits the highest ionic conductivity (2.83×10^{-5} S/cm), which therefore was chosen as the study subject in the following research. LLZO with different coating ratios of coupling agent was composted with PEO to obtain composite electrolyte. The Nyquist plots of the composite electrolyte in Figure 3c demonstrated the coupling agent coating effectively improved the ionic conductivity of the composite electrolyte. Furthermore, the calculated ionic conductivity (Figure 3d) revealed that KLP with a 2 wt.% coupling agent presents the highest ionic conductivity (7.29×10^{-5} S/cm), almost three times of the pristine PLP sample, which confirms that the well-dispersed K−LLZO particles are quite effective in enhancing the ionic conductivity of the composite electrolyte than the agglomerates, which further demonstrates the positive effect of silane coupling agent coating on LLZO for improving LLZO-based composite electrolytes.

Moreover, the LSV measurement was carried out to investigate whether the introduction of a coupling agent would narrow the electrochemical window (Figure 3e). Compared with PLP, the addition of a silane coupling agent has no obvious effect on the electrochemical window of KLP, which indicates the coupling agent exhibits superior anti-oxidative stability, and surface modification with a silane coupling agent shows the possibility of being applicable to surface modification of more materials, such as improving adhesive performance between high-voltage cathode materials and polymer binders.

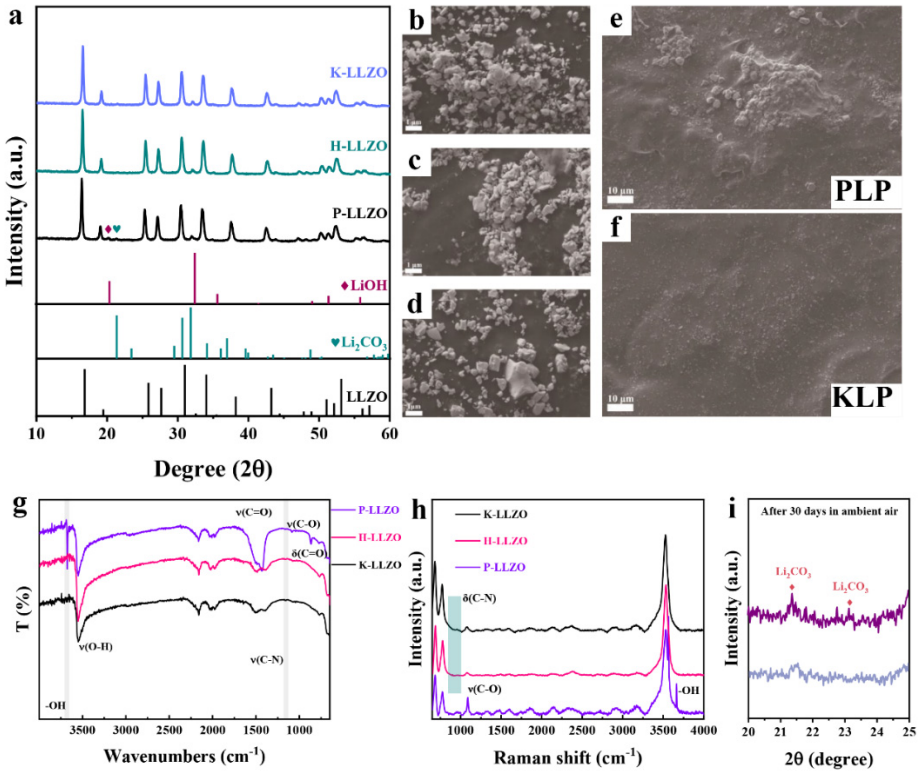

Figure 2. (**a**) XRD patterns of each LLZO powder; Particle SEM morphology (**b**) P−LLZO, (**c**) H−LLZO, (**d**) K−LLZO; Composite solid electrolyte SEM morphology (**e**) P−LLZO@PEO (PLP), (**f**) K−LLZO@PEO (KLP); (**g**) FTIR and (**h**) Raman spectra of different LLZO powders; (**i**) Enlarged XRD patterns of K−LLZO (the curve above) and H−LLZO (the curve below) after 30 days in ambient air.

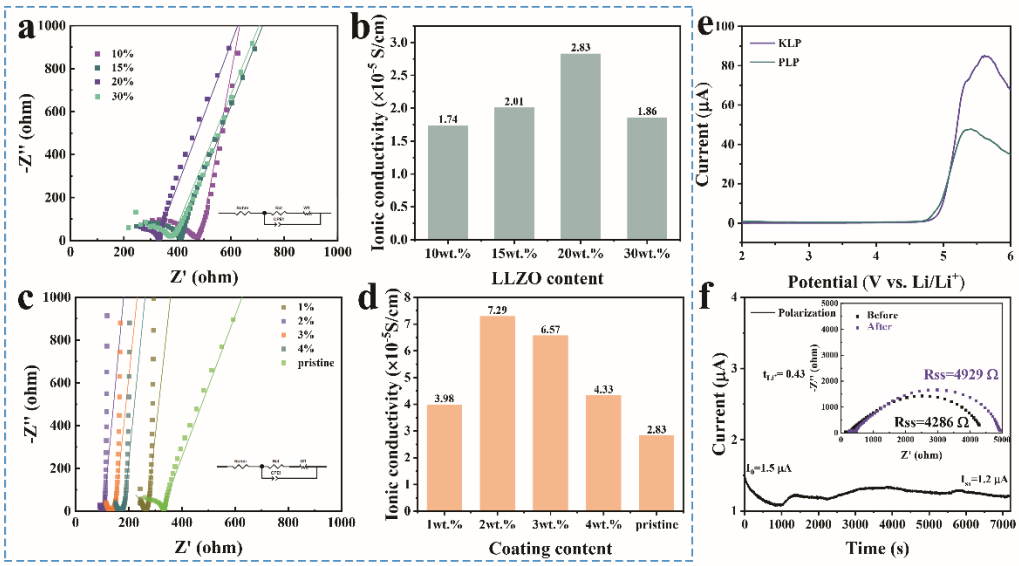

Figure 3. (**a**) Nyquist plots of PLP with different P−LLZO filler contents; (**b**) Room temperature calculated ionic conductivity of PLP with different filler ratios; (**c**) Nyquist plots of KLP coated with different coupling agent ratio; (**d**) Room temperature calculated ionic conductivity of KLP coated with different coupling agent ratio; (**e**) Linear sweep voltammetry (LSV) curves of KLP and PLP; (**f**) KLP lithium-ion transfer number (The inset is the impedance before and after polarization).

In addition, the Li-ion transference number (T_{Li}^+) is also a critical factor of composite electrolytes. A high T_{Li}^+ is beneficial for SSEs to enable smooth Li^+ flux and suppress Li dendrites growth [35]. Generally, polymer-based electrolytes show a low T_{Li}^+ due to the

free anions from the decomposition of the Li salt. The free anions form a space charge near the Li anodes when the electrolyte is biased, which hinders the uniform deposition of Li^+. Therefore, Li dendrites grow and may eventually cause short circuits of cells. As illustrated in Figure 3f, the calculated $T_{Li}{}^+$ of KLP is 0.43, which is almost twice of pure PEO(LiTFSI) (~0.21) [22]. the K−LLZO enhanced composite electrolyte exhibits increased $T_{Li}{}^+$ due to the Lewis acid surface of fresh LLZO immobilized anions [36]. In addition, the well-dispersed K−LLZO has exposed a more active Lewis acid surface, which further increases the Li-ion concentration and ionic conductivity by promoting the dissociation of Li salt and immobilizing more anions of Li salt [37]. Since the modified KLP exhibits high ionic conductivity and $T_{Li}{}^+$, it is inferred that KLP may be feasible to inhibit the growth of lithium dendrites as well as enhance battery performance.

Considering that the high $T_{Li}{}^+$ of KLP electrolytes is beneficial for uniform lithium deposition, Li/KLP/Li and Li/PLP/Li symmetric cells were assembled to investigate the dendrite suppression capabilities. As illustrated in Figure 4a, a soft short circuit phenomenon occurred in Li/PLP/Li symmetric cells when cycling at a current density of 0.3 mA/cm^2 (Figure 4b). Furthermore, a symmetric cell with PLP electrolyte exhibits frequent soft short circuits and extremely large polarization voltage (750 mV) at a current density of 0.5 mA/cm^2 (Figure 4c), which suggests the poor lithium dendrites suppression capabilities and inferior interfacial stability between PLP and Li metal anode [38]. In contrast, even at a current density as high as 0.5 mA/cm^2 under a capacity density of 0.5 mA h/cm^2, Li/KLP/Li symmetric cells exhibit excellent cycling stability (~200 mV overpotential) without obviously short circuit, indicating enhanced interfacial stability and stable Li^+ plating/stripping behaviors. In general, lithium dendrites usually result from inhomogeneous and localized currents. The aggregated LLZTO particles caused localized currents due to the conductivity difference between LLZTO and PEO, which leads to the short circuit [26]. Therefore, the stable cycle of Li/KLP/Li may attribute to well dispersed LLZTO in the polymer matrix and high $T_{Li}{}^+$ which leads to homogeneous lithium ions flow and current. This is also verified by the surface morphology SEM images of the lithium anode after cycling (Figure 4d). The Li metal anode of the Li/PLP/Li cell shows the mossy-like dendrite morphologies on the surface, which represents an uneven lithium-ion deposition behavior. On the contrary, the Li metal anode of the Li/KLP/Li cell shows a smooth surface, revealing that the K−LLZO enhanced PEO composite electrolyte ensures a uniform lithium deposition.

To further evaluate the feasibility of KLP for practical applications, LFP/Li all-solid-state batteries with KLP and PLP were assembled. As presented in Figure 5a, LFP/KLP/Li cells exhibit a high initial specific discharge capacity of ~155 mA h/g at 60 °C and 0.1 C with 94% capacity retention after 70 cycles. While the counter LFP/PLP/Li cells displayed only ~70% capacity retention under the same conditions, which demonstrates the enhanced positive effect of the coupling agent modified LLZTO in PEO composite electrolyte. Moreover, as shown in Figure 5b, the assembled LFP/Li all-solid-state batteries with KLP obtained superior cycling stability even at room temperature (almost no decay after 60 cycles). Moreover, with the introduction of K−LLZO, LFP/KLP/Li presents almost 100% columbic efficiency at 60 °C and 25 °C, which further verified the introduction of K−LLZO improved cycling stability. Importantly, the cycling performance of $LiFePO_4$/SCE/Li cell is superior to those reported in previous literature (Supplementary Material Table S1). Our designed facile and cost-effective coupling agent-modified garnet fillers demonstrate great promise for upgrading composite electrolytes.

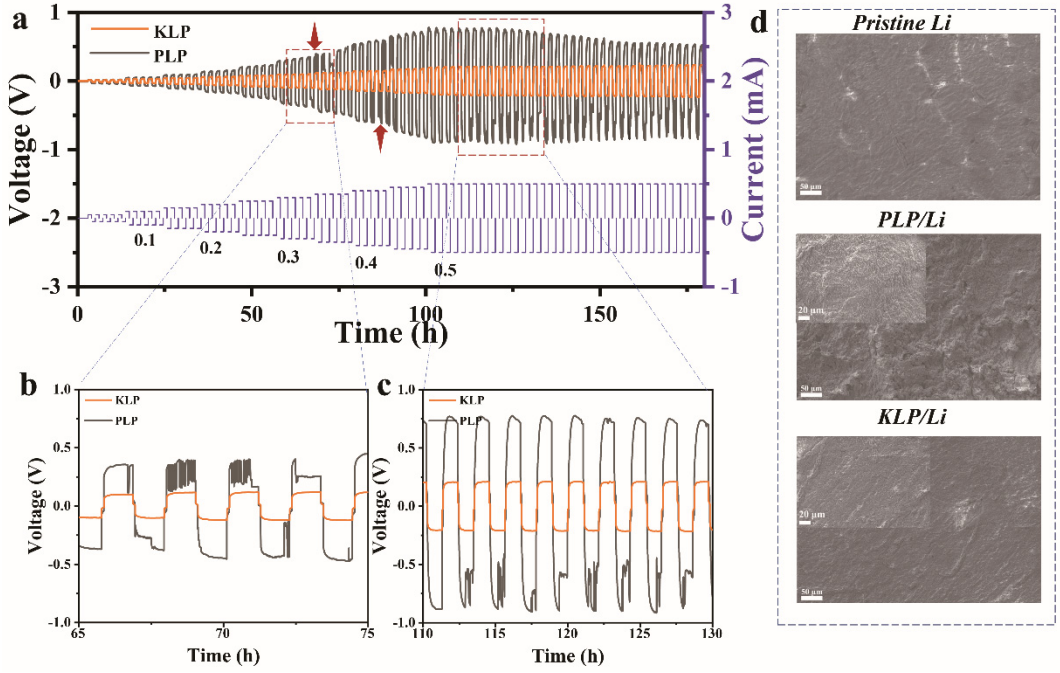

Figure 4. (**a**) Room temperature cycling performance of Li/KLP/Li and Li/PLP/Li lithium symmetric batteries at different current densities; (**b**) Enlarged plots at 0.3 mA/cm^2 current density; (**c**) Enlarged plots at 0.5 mA/cm^2 current density; (**d**) SEM topography of the initial lithium metal surface.

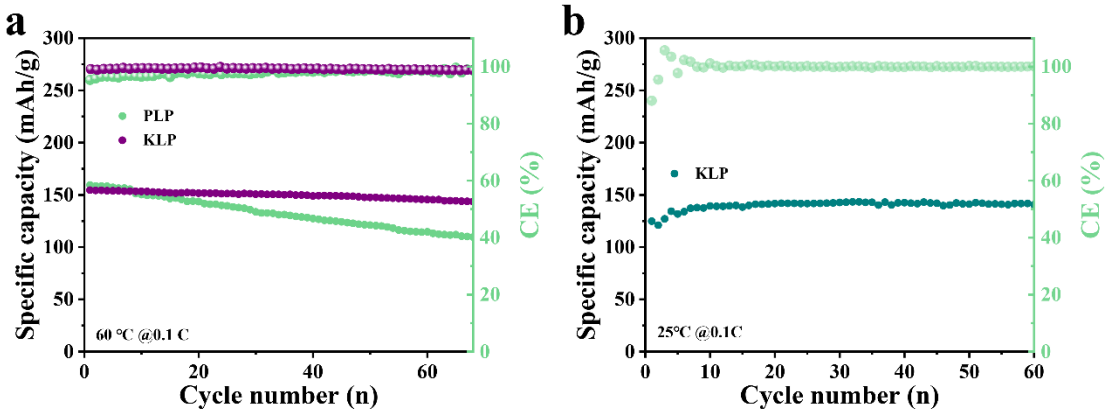

Figure 5. (**a**) Cycling performance of LFP/PLP/Li and LFP/KLP/Li cells at 60 °C; (**b**) Cycling performance of LFP/Li cells at room temperature (25 °C).

3. Conclusions

In summary, the garnet coated with a cost-effective silane coupling agent proved highly effective in elevating its dispersion in the polymer matrix and air stability. Furthermore, the obtained composite solid electrolytes deliver greatly improved battery performance. Compared with PLP, KLP shows almost 3 times improved ionic conductivity of 7.2×10^{-5} S/cm at room temperature due to the enhanced Li^+ transport at the interface. A high T_{Li^+} of 0.43 is achieved in the KLP due to the anions immobilized on the exposed Lewis-acid fresh LLZO surface. The Li/KLP/Li cells can operate at 0.5 mA/cm^2 and exhibit a smooth lithium anode morphology after cycling owing to the well-dispersed K−LLZO particles and uniform Li^+ flux. Our coating method with a silane coupling agent can be extended to improve the dispersion of inorganic fillers in the polymer matrix in other composite solid electrolytes or high-voltage composite cathodes, which paves the way to upgrade the SSEs and promote the commercial application of SSBs.

3.1. Experimental

3.1.1. Hydrochloric Acid Treatment of P−LLZO

P−LLZO (500 nm, Hefei Kejing Material Technology Co., Ltd., Hefei, China) powders were first dispersed in an appropriate amount of anhydrous ethanol. 1 M hydrochloric acid solution (Sinopharm Chemical Reagent Co., Ltd., Shanghai, China) was added to the above-mentioned suspension followed by ultrasonic dispersion for 30 s to remove Li_2CO_3 on the surface of the P−LLZO. Then the hydrochloric acid concentration was diluted with ~250 mL of deionized water to prevent the hydrochloric acid solution from reacting with LLZO. The obtained suspension was washed with deionized water and anhydrous ethanol three times and then dried at a 60 °C-vacuum oven for 12 h to obtain the H−LLZO.

3.1.2. The Preparation of K−LLZO

1 wt.%, 2 wt.%, 3 wt.%, and 4 wt.% of the H−LLZO silane coupling agent KH550 (Aladdin, 99%) and H−LLZO powders were first dispersed in anhydrous ethanol to obtain suspensions. Then, the appropriate amount of deionized water was added to the above suspensions to promote the hydrolysis of the silane coupling agent. After further magnetic stirring for 30 min, the obtained suspension was centrifuged and washed with anhydrous ethanol three times. The K−LLZO was acquired after drying in a vacuum oven at 60 °C for 12 h.

3.1.3. Fabrication of the Composite Electrolytes

P−LLZO and K−LLZO particles with various concentrations were added into acetonitrile and dispersed by sonication. After that, PEO and LiTFSI (EO/Li = 12:1 by mol) were added to the solution and vigorously stirred overnight. Then, the homogenized solution was poured into a polytetrafluoroethylene module. The composite electrolyte membranes were obtained after drying in a vacuum oven for 12 h. All procedures were processed in an argon-filled glove box with H_2O and O_2 levels below 0.1 ppm.

3.1.4. Characterizations of Materials Properties

The X-ray diffraction (XRD) patterns were measured in an angular range of 10–80° with an X-ray diffractometer (PANalytical/Aeris, Cu K_α radiation (λ = 0.154 nm)) at a power of 40 kV. The morphology images were recorded by a scanning electron microscope (SEM, ZEISS, Crossbeam350). The Fourier transform infrared (FTIR) spectra were performed on a BRUKER TENSOR 37. The Raman spectra were characterized on Renishaw InVia.

3.1.5. Electrochemical Characterization of Composite Electrolytes

Electrochemical impedance spectroscopy (EIS) tests of stainless steel (SS)/SSEs/SS blocked cells were performed on the CHI660E electrochemical station in a frequency range from 1 MHz to 0.1 Hz using 10 mV amplitude. LSV measurements of Li/composite electrolyte/SS were recorded in a voltage range from open circuit voltage to 6 V on a CHI660E electrochemical station at room temperature with a 0.1 mV s^{-1} scan rate. Galvanostatic cycling of lithium symmetric cells was conducted by the LAND 2001A battery testing system at various current densities. LFP/Li 2032-type coin cells were assembled to investigate the electrochemical performance of cells. Typically, active materials, super P, and PVDF binder were dispersed in *N*-methyl-2-pyrrolidone with a weight ratio of 8:1:1, followed by casting on Al foil with a doctor blade, and then further dried at 110 °C vacuum drying oven overnight. The mass loading of cathode active material was about 2 mg/cm^2. The LFP/Li cells were operated at voltage ranges of 2.5–3.8 V at 25 and 60 °C.

Supplementary Materials: The following supporting information can be downloaded at: https://www.mdpi.com/article/10.3390/batteries8100141/s1, Figure S1. SEM image of K−LLZO and corresponding Ta, Zr, and Si element EDS mapping images. Figure S2. XRD patterns of K−LLZO and H−LLZO after one month exposure to air. Table S1. Comparation of energy storage property with the reported literatures. Table S2. Equivalent circuit fitting value.

Author Contributions: Conceptualization, J.C.; Formal analysis, J.C. and H.Z.; Funding acquisition, D.L. and L.C.; Investigation, J.C. and H.Z.; Methodology, J.C., H.Z. and Y.L.; Project administration, H.Z., D.L. and L.C.; Resources, J.C., H.Z., Z.Z. and L.C.; Supervision, D.L. and L.C.; Validation, H.Z.; Visualization, J.C.; Writing—original draft, J.C.; Writing—review & editing, J.C., H.Z., D.L., Y.L., Z.Z., F.J., Y.W., X.X., Q.S., S.W., J.L. and L.C. All authors have read and agreed to the published version of the manuscript.

Funding: This research was funded by School Research Startup Expenses of Harbin Institute of Technology (Shenzhen): DD29100027; School Research Startup Expenses of Harbin Institute of Technology (Shenzhen): DD45001022; National Natural Science Foundation of China: 52002094; Guangdong Basic and Applied Basic Research Foundation: 2019A1515110756; Shenzhen Science and Technology Program: JCYJ20210324121411031; Shenzhen Science and Technology Program: JSGG20210802125380401 4; Shenzhen Science and Technology Program: RCBS20210706092218040; The Open Fund of the Guangdong Provincial Key Laboratory of Advanced Energy Storage materials: asem202107; the Foundation of State Key Laboratory of High-efficiency Utilization of Coal and Green Chemical Engineering: 2022-K16; State Key Laboratory of Advanced Welding and Joining, School of materials Science and Engineering, Harbin Institute of Technology: HX20200170.

Informed Consent Statement: Not applicable.

Data Availability Statement: Data sharing not applicable.

Conflicts of Interest: The authors declare no conflict of interest.

References

1. Fan, L.-Z.; He, H.; Nan, C.-W. Tailoring inorganic–polymer composites for the mass production of solid-state batteries. *Nat. Rev. Mater.* **2021**, *6*, 1003–1019. [CrossRef]
2. Sarkar, S.; Thangadurai, V. Critical Current Densities for High-Performance All-Solid-State Li-Metal Batteries: Fundamentals, Mechanisms, Interfaces, Materials, and Applications. *ACS Energy Lett.* **2022**, *7*, 1492–1527. [CrossRef]
3. Schnell, J.; Knörzer, H.; Imbsweiler, A.J.; Reinhart, G. Solid versus Liquid—A Bottom-Up Calculation Model to Analyze the Manufacturing Cost of Future High-Energy Batteries. *Energy Technol.* **2020**, *8*, 1901237. [CrossRef]
4. Tan, S.J.; Wang, W.P.; Tian, Y.F.; Xin, S.; Guo, Y.G. Advanced Electrolytes Enabling Safe and Stable Rechargeable Li-Metal Batteries: Progress and Prospects. *Adv. Funct. Mater.* **2021**, *31*, 2105253. [CrossRef]
5. Thangadurai, V.; Narayanan, S.; Pinzaru, D. Garnet-type solid-state fast Li ion conductors for Li batteries: Critical review. *Chem. Soc. Rev.* **2014**, *43*, 4714–4727. [CrossRef] [PubMed]
6. Zhang, M.; Huang, Z.; Cheng, J.; Yamamoto, O.; Imanishi, N.; Chi, B.; Pu, J.; Li, J. Solid state lithium ionic conducting thin film $Li_{1.4}Al_{0.4}Ge_{1.6}(PO_4)_3$ prepared by tape casting. *J. Alloys Compd.* **2014**, *590*, 147–152. [CrossRef]
7. Wang, C.; Fu, K.; Kammampata, S.P.; McOwen, D.W.; Samson, A.J.; Zhang, L.; Hitz, G.T.; Nolan, A.M.; Wachsman, E.D.; Mo, Y.; et al. Garnet-Type Solid-State Electrolytes: Materials, Interfaces, and Batteries. *Chem. Rev.* **2020**, *120*, 4257–4300. [CrossRef] [PubMed]
8. Tan, D.H.S.; Chen, Y.T.; Yang, H.; Bao, W.; Sreenarayanan, B.; Doux, J.M.; Li, W.; Lu, B.; Ham, S.Y.; Sayahpour, B.; et al. Carbon-free high-loading silicon anodes enabled by sulfide solid electrolytes. *Science* **2021**, *373*, 1494–1499. [CrossRef] [PubMed]
9. Yoshima, K.; Harada, Y.; Takami, N. Thin hybrid electrolyte based on garnet-type lithium-ion conductor $Li_7La_3Zr_2O_{12}$ for 12 V-class bipolar batteries. *J. Power Sources* **2016**, *302*, 283–290. [CrossRef]
10. Liu, Q.; Geng, Z.; Han, C.; Fu, Y.; Li, S.; He, Y.-B.; Kang, F.; Li, B. Challenges and perspectives of garnet solid electrolytes for all solid-state lithium batteries. *J. Power Sources* **2018**, *389*, 120–134. [CrossRef]
11. Naseer, M.A.; Tufail, M.K.; Ali, A.; Hussain, S.; Khan, U.; Jin, H.B. Review on Computational-Assisted to Experimental Synthesis, Interfacial Perspectives of Garnet-Solid Electrolytes for All-Solid-State Lithium Batteries. *J. Electrochem. Soc.* **2021**, *168*, 060529. [CrossRef]
12. Liu, X.-Z.; Ding, L.; Liu, Y.-Z.; Xiong, L.-P.; Chen, J.; Luo, X.-L. Room-temperature ionic conductivity of Ba, Y, Al co-doped $Li_7La_3Zr_2O_{12}$ solid electrolyte after sintering. *Rare Met.* **2021**, *40*, 2301–2306. [CrossRef]
13. Ohta, S.; Kobayashi, T.; Seki, J.; Asaoka, T. Electrochemical performance of an all-solid-state lithium ion battery with garnet-type oxide electrolyte. *J. Power Sources* **2012**, *202*, 332–335. [CrossRef]
14. Kim, K.J.; Rupp, J.L.M. All ceramic cathode composite design and manufacturing towards low interfacial resistance for garnet-based solid-state lithium batteries. *Energy Environ. Sci.* **2020**, *13*, 4930–4945. [CrossRef]
15. Liu, T.; Ren, Y.; Shen, Y.; Zhao, S.-X.; Lin, Y.; Nan, C.-W. Achieving high capacity in bulk-type solid-state lithium ion battery based on $Li_{6.75}La_3Zr_{1.75}Ta_{0.25}O_{12}$ electrolyte: Interfacial resistance. *J. Power Sources* **2016**, *324*, 349–357. [CrossRef]
16. Chen, S.; Zhang, J.; Nie, L.; Hu, X.; Huang, Y.; Yu, Y.; Liu, W. All-Solid-State Batteries with a Limited Lithium Metal Anode at Room Temperature using a Garnet-Based Electrolyte. *Adv. Mater.* **2020**, *33*, 2002325. [CrossRef] [PubMed]

17. Duan, H.; Chen, W.P.; Fan, M.; Wang, W.P.; Yu, L.; Tan, S.J.; Chen, X.; Zhang, Q.; Xin, S.; Wan, L.J.; et al. Building an Air Stable and Lithium Deposition Regulable Garnet Interface from Moderate-Temperature Conversion Chemistry. *Angew. Chem. Int. Ed. Engl.* **2020**, *59*, 12069–12075. [CrossRef] [PubMed]
18. Sharafi, A.; Kazyak, E.; Davis, A.L.; Yu, S.; Thompson, T.; Siegel, D.J.; Dasgupta, N.P.; Sakamoto, J. Surface Chemistry Mechanism of Ultra-Low Interfacial Resistance in the Solid-State Electrolyte $Li_7La_3Zr_2O_{12}$. *Chem. Mater.* **2017**, *29*, 7961–7968. [CrossRef]
19. Rosen, M.; Ye, R.; Mann, M.; Lobe, S.; Finsterbusch, M.; Guillon, O.; Fattakhova-Rohlfing, D. Controlling the lithium proton exchange of LLZO to enable reproducible processing and performance optimization. *J. Mater. Chem. A* **2021**, *9*, 4831–4840. [CrossRef]
20. Huo, H.; Luo, J.; Thangadurai, V.; Guo, X.; Nan, C.-W.; Sun, X. Li_2CO_3: A Critical Issue for Developing Solid Garnet Batteries. *ACS Energy Lett.* **2019**, *5*, 252–262. [CrossRef]
21. Lopez, J.; Pei, A.; Oh, J.Y.; Wang, G.-J.N.; Cui, Y.; Bao, Z. Effects of Polymer Coatings on Electrodeposited Lithium Metal. *J. Am. Chem. Soc.* **2018**, *140*, 11735–11744. [CrossRef]
22. Huo, H.; Li, X.; Sun, Y.; Lin, X.; Doyle-Davis, K.; Liang, J.; Gao, X.; Li, R.; Huang, H.; Guo, X.; et al. Li_2CO_3 effects: New insights into polymer/garnet electrolytes for dendrite-free solid lithium batteries. *Nano Energy* **2020**, *73*, 104836. [CrossRef]
23. Gupta, A.; Sakamoto, J. Controlling Ionic Transport through the PEO-LiTFSI/LLZTO Interface. *Electrochem. Soc. Interface* **2019**, *28*, 63–69. [CrossRef]
24. Lee, M.J.; Shin, D.O.; Kim, J.Y.; Oh, J.; Kang, S.H.; Kim, J.; Kim, K.M.; Lee, Y.M.; Kim, S.O.; Lee, Y.-G. Interfacial barrier free organic-inorganic hybrid electrolytes for solid state batteries. *Energy Storage Mater.* **2021**, *37*, 306–314. [CrossRef]
25. Jia, M.; Zhao, N.; Bi, Z.; Fu, Z.; Xu, F.; Shi, C.; Guo, X. Polydopamine-Coated Garnet Particles Homogeneously Distributed in Poly(propylene carbonate) for the Conductive and Stable Membrane Electrolytes of Solid Lithium Batteries. *ACS Appl. Mater. Interfaces* **2020**, *12*, 46162–46169. [CrossRef]
26. Huang, Z.; Pang, W.; Liang, P.; Jin, Z.; Grundish, N.; Li, Y.; Wang, C.-A. A dopamine modified $Li_{6.4}La_3Zr_{1.4}Ta_{0.6}O_{12}$/PEO solid-state electrolyte: Enhanced thermal and electrochemical properties. *J. Mater. Chem. A* **2019**, *7*, 16425–16436. [CrossRef]
27. Yan, C.; Zhu, P.; Jia, H.; Du, Z.; Zhu, J.; Orenstein, R.; Cheng, H.; Wu, N.; Dirican, M.; Zhang, X. Garnet-rich composite solid electrolytes for dendrite-free, high-rate, solid-state lithium-metal batteries. *Energy Storage Mater.* **2020**, *26*, 448–456. [CrossRef]
28. Li, Y.; Xu, B.; Xu, H.; Duan, H.; Lu, X.; Xin, S.; Zhou, W.; Xue, L.; Fu, G.; Manthiram, A.; et al. Hybrid Polymer/Garnet Electrolyte with a Small Interfacial Resistance for Lithium-Ion Batteries. *Angew. Chem. Int. Ed. Engl.* **2017**, *56*, 753–756. [CrossRef]
29. Lv, J.-S.; Guo, S.-K.; He, Y.-B. Modification strategies of $Li_7La_3Zr_2O_{12}$ ceramic electrolyte for high-performance solid-state batteries. *Tungsten* **2021**, *3*, 260–278. [CrossRef]
30. Huo, H.; Chen, Y.; Zhao, N.; Lin, X.; Luo, J.; Yang, X.; Liu, Y.; Guo, X.; Sun, X. In-situ formed Li_2CO_3-free garnet/Li interface by rapid acid treatment for dendrite-free solid-state batteries. *Nano Energy* **2019**, *61*, 119–125. [CrossRef]
31. Cheng, Z.; Liu, T.; Zhao, B.; Shen, F.; Jin, H.; Han, X. Recent advances in organic-inorganic composite solid electrolytes for all-solid-state lithium batteries. *Energy Storage Mater.* **2021**, *34*, 388–416. [CrossRef]
32. Fan, P.; Liu, H.; Marosz, V.; Samuels, N.T.; Suib, S.L.; Sun, L.; Liao, L. High Performance Composite Polymer Electrolytes for Lithium-Ion Batteries. *Adv. Funct. Mater.* **2021**, *31*, 2101380. [CrossRef]
33. Horowitz, Y.; Lifshitz, M.; Greenbaum, A.; Feldman, Y.; Greenbaum, S.; Sokolov, A.P.; Golodnitsky, D. Review—Polymer/Ceramic Interface Barriers: The Fundamental Challenge for Advancing Composite Solid Electrolytes for Li-Ion Batteries. *J. Electrochem. Soc.* **2020**, *167*, 160514. [CrossRef]
34. Xie, Y.; Hill, C.A.S.; Xiao, Z.; Militz, H.; Mai, C. Silane coupling agents used for natural fiber/polymer composites: A review. *Compos. Part A Appl. Sci. Manuf.* **2010**, *41*, 806–819. [CrossRef]
35. Huo, H.; Wu, B.; Zhang, T.; Zheng, X.; Ge, L.; Xu, T.; Guo, X.; Sun, X. Anion-immobilized polymer electrolyte achieved by cationic metal-organic framework filler for dendrite-free solid-state batteries. *Energy Storage Mater.* **2019**, *18*, 59–67. [CrossRef]
36. Zhang, J.; Zhao, N.; Zhang, M.; Li, Y.; Chu, P.K.; Guo, X.; Di, Z.; Wang, X.; Li, H. Flexible and ion-conducting membrane electrolytes for solid-state lithium batteries: Dispersion of garnet nanoparticles in insulating polyethylene oxide. *Nano Energy* **2016**, *28*, 447–454. [CrossRef]
37. Guo, Y.; Cheng, J.; Zeng, Z.; Li, Y.; Zhang, H.; Li, D.; Ci, L. Li_2CO_3: Insights into Its Blocking Effect on Li-Ion Transfer in Garnet Composite Electrolytes. *ACS Appl. Energy Mater.* **2022**, *5*, 2853–2861. [CrossRef]
38. Cheng, J.; Hou, G.; Chen, Q.; Li, D.; Li, K.; Yuan, Q.; Wang, J.; Ci, L. Sheet-like garnet structure design for upgrading PEO-based electrolyte. *Chem. Eng. J.* **2022**, *429*, 132343. [CrossRef]